Axial compressive behaviours of steel–concrete-steel sandwich composite walls with novel enhanced C-channels

Jia-Bao Yan, Anzhen Chen, Tao Wang

▶ **To cite this version:**

Jia-Bao Yan, Anzhen Chen, Tao Wang. Axial compressive behaviours of steel–concrete-steel sandwich composite walls with novel enhanced C-channels. Structures, 2020, 28, pp.407 - 423. ⟨10.1016/j.istruc.2020.08.070⟩. ⟨hal-03492485⟩

HAL Id: hal-03492485

https://hal.science/hal-03492485v1

Submitted on 14 Sep 2022

HAL is a multi-disciplinary open access archive for the deposit and dissemination of scientific research documents, whether they are published or not. The documents may come from teaching and research institutions in France or abroad, or from public or private research centers.

L'archive ouverte pluridisciplinaire **HAL**, est destinée au dépôt et à la diffusion de documents scientifiques de niveau recherche, publiés ou non, émanant des établissements d'enseignement et de recherche français ou étrangers, des laboratoires publics ou privés.

Distributed under a Creative Commons CC BY-NC 4.0 - Attribution - Non-commercial use - International License

Version of Record: https://www.sciencedirect.com/science/article/pii/S2352012420304604
Manuscript_3891d68e49cb785cbc6b9ffc20c5a495

Axial compressive behaviours of steel-concrete-steel sandwich composite walls with novel enhanced C-channels

Jia-Bao Yan[1,2], Anzhen Chen[2], Tao Wang[3,*]

[1]*Key Laboratory of Coast Civil Structure Safety of Ministry of Education, Tianjin University, Tianjin 300350, China*
[2]*School of Civil Engineering, Tianjin University, Tianjin 300350, China*
[3]*Key Laboratory of Earthquake Engineering and Engineering Vibration, Institute of Engineering Mechanics, CEA, Harbin 150080, China*

Abstract: This paper developed novel steel-concrete-steel sandwich composite walls (SCSSCWs) with enhanced C-channels (SCSSCW-ECs), and studied their compressive behaviours through seven axial compression tests. The studied parameters include layout of C-channels in SCSSCWs, faceplate thickness, strength of concrete core, vertical and horizontal spacing of C-channels. Test results exhibited a three-stage working mechanism for SCSSCW-ECs under compression. Experimental observations also showed that SCSSCW-ECs exhibited concrete core crushing and local buckling of faceplate. The test results also offer useful information on the mechanism and influences of these studied parameters on axial compressive behaviours of novel SCSSCW-ECs. The layout of novel ECs in the SCSSCW-ECs was finally optimized including layout of C-channels as well as their spacing. This paper also developed theoretical models and modified code equations in AISC, CECS, and Eurocode 4 to estimate ultimate compressive resistance of SCSSCW-ECs. These models have been validated by reported 11 test results. The validations showed that developed theoretical models offered the most accurate predictions on ultimate compressive resistance of SCSSCW-ECs.

Keywords: Composite wall; steel-concrete-steel sandwich structure; compression test; shear connectors; analytical models; C-channel; shear wall.
***Corresponding author**: Tao Wang, E-mail address: wangtao@iem.ac.cn

© 2020 published by Elsevier. This manuscript is made available under the CC BY NC user license
https://creativecommons.org/licenses/by-nc/4.0/

Nomenclature

A_c=Cross-sectional area of concrete core
A_s= Cross-sectional area of faceplate
A_{sb}= Cross-sectional area of bolt
A_{sc}= Cross-sectional area of web of C-channel
$A_{s,Ai}$,$B_{s,Bj}$,$C_{s,Ck=}$ Width of the A, B and C strip of faceplates in Fig. 11
E_c=Modulus of elasticity of concrete
E_s=Elastic modulus of steel
$(EI)_{eff}$= Effective flexural stiffness
E_{s1}, E_{s2} =Modulus of elasticity for steel faceplate and C-channels
I_c = Moment inertia of concrete section
I_s = Moment inertia of steel faceplate
K_e=Initial stiffness
K = Boundary condition coefficient
L=Laterally unbraced length of the member
L_c= Length of C-channel flange
N_0 =nominal compressive strength of zero length, axially loaded composite member
N_c =Compressive resistance of concrete core
N_{cr} = elastic critical buckling force
N_s =Compressive resistance of steel faceplate
N_T,N_{uA},N_E,$N_{CN=}$ Predicted ultimate compressive resistance of SCSSCW-ECs by theoretical models, AISC, Eurocode 4 and CECS, respectively
P_e= Elastic limit load
$P_{u=}$ Experimental ultimate compressive resistance of SCSSCW-ECs
S_h = Horizontal spacing of C-channels
S_v = Vertical spacing of C-channels
S_{va}, S_{ha}= Average vertical and horizontal spacing of C-channels
T_c= Tensile resistance of C-channels
T_{cs}= Tensile resistance of C-channel web
T_{cb}= Tensile resistance of anchoring bolt
f_c, f_{cu} = Cylindrical and cubic compressive strength of concrete, respectively
f_y , f_u =Yield and ultimate strength of steel faceplate, respectively
t_s = Faceplate thickness
t_c = Concrete thickness
Δ_u=Shortening at P_u
$\Delta_{85\%}$=Shortening at 85% P_u during recession stage
α_s= Coefficient, and herein equals to 0.19
λ= Slenderness ratio, and equals to S_{va}/t_s
λ_0 = Generalized slenderness ratio
χ = reduction factor for flexural buckling
φ = stability coefficient
η= Buckling length coefficient
$\bar{\sigma}_c$ = Average compressive stress
σ_{cc}= Average compressive stress of concrete core confined by the steel skeleton
σ_{cf}= Confining stress on concrete core by steel skeleton
$\sigma_{cr,}$ = Critical buckling stress
σ_y, σ_u =Yield and ultimate strength of C-channels, respectively
σ_{uc}= tensile strength of C-channel
σ_{ub}= tensile strength of anchoring bolt

Abbreviations

CC, concrete crushing; COV, coefficient of variation; CS, concrete splitting; DI, ductility index; EC, enhanced C-channel; LVDT, linear varying displacement transducer; SCSSCW-EC, SCSSCWs with ECs; SCSSCW, steel-concrete-steel sandwich composite wall; TM, theoretical models.

1 Introduction

Recently, steel-concrete-steel sandwich composite walls (SCSSCWs) become popular and have been put into use as shear walls in high-rise buildings [1-3], nuclear shielding walls [4-5], immersed tunnels [6-7], protective structures [8-9], and ice walls [10-12]. The representative form of SCSSCWs usually has two external steel faceplates and a sandwiched concrete core, which uses adhesive materials or connectors to bond them together as a composite structure. Compared with the traditional reinforced concrete walls, the SCSSCWs possess advantages of savings on formwork and labours force for concrete casting, increased fabrication efficiency, offering impermeable face skin, and high structural performances under static and dynamic loadings [13]. Compared with steel structure [14-15], SCSSCWs can be also used in prefabrication construction with the improved fire and corrosion resistance.

From the view of improvements on bonding at steel-concrete interface, SCSSCWs with shear connectors have been proposed. Ji et al. [1] adopted the bolts through the depth of SCSSCWs that directly connected the two faceplates as shown in Fig. 1(a). Followed cyclic tests on the full size SCSSCWs with this type of connectors proved its bonding effectiveness on the seismic performances of sandwich walls [1-2]. However, the through bolts in SCSSCWs required amounts of openings in steel faceplates that compromised the strength of faceplates, and complex the fabrication procedures of SCSSCWs. Headed studs have also been extensively used in SCSSCWs as the steel-concrete bonding measures as shown in Fig. 1(b). Nie et al. [3], Zhang et al. [4], Choi et al. [16-17] adopted short headed studs to achieve the

concrete-faceplate bonding in SCSSCWs. In some cases, the tying bars were used accompanied with these short headed studs [3, 18] to improve the outward separation resistance between the concrete core and steel faceplates. Yan et al. [11, 19] further simplified this bonding and adopted headed studs with overlapped length instead of tying bars in SCSSCWs. And the cyclic tests on the SCSSCWs with overlapped studs improved the effectiveness of this type of bonding. However, the steel-concrete bonding provided by the overlapped studs greatly depends on integrity of their embedded concrete core. Once the concrete core is damaged, the SCSSCWs would lose their composite actions as well as their load carrying capacities. Xie et al. [20] proposed a strong bonding method for SCSSCWs that directly connects the two external faceplates using friction-welded straight bars [see Fig. 1(c)]. Previous extensive studies [20-22] proved the effectiveness of this direct bonding measure. However, the depth of SCSSCWs using friction-welded straight bars is limited by the fabrication equipment in a range of 0.2~0.7 m. Double J-hooks, as shown in Fig. 1(d), could overcome this disadvantage [10] and have been proposed for SCSSCWs by Liew et al. [23]. The full-scale tests proved the excellent performances of SCSSCWs with double J-hooks under axial compression [10, 12] and horizontal cyclic loads [24-25]. However, the tensile separation resistance of double J-hooks is still partially affected by their embedment in the concrete core. Qin et al. [26-27] proposed the wave-bar connectors for SCSSCWs. This type of connectors directly connected the two external steel faceplates using the wave-shaped bars. However, fabrication difficulties exist for welding this connecting system inside the limited space of steel

skeleton formed by two external steel faceplates. More recently, Yan et al. [28] proposed a new type of SCSSCWs with novel enhanced C-channels (ECs) [see Fig. 1(e)]. This type of ECs adopted the C-channels with one flange welded to the steel faceplate and the other flange externally bolt connected to the opposite faceplate. Fig. 1(f) shows the fabrication procedures of ECs in SCSSCWs. This type of new connectors could offer relative high shear and tensile resistances at the faceplate-concrete interface. Preliminary prototype tests have been performed to check the axial compressive behaviours of SCSSCWs with ECs (SCSSCW-ECs) [28]. Thus, it is of interest to make more comprehensive studies on the axial compressive behaviours of SCSSCW-ECs.

Due to excellent composite effect of steel and concrete, SUSSCW-ECs can be used as the main walls in high-rise building and other vertical load-bearing members. This paper contributes to comprehensive understanding on axial compressive behaviours of SCSSCW-ECs. Firstly, axial compression tests were carried out on eight SCSSCW-ECs. The studied parameters included layout of C-channels in SCSSCWs (i.e., C-channels with their webs in horizontal or vertical direction), faceplate thickness (t_s), strength of concrete core (f_c), vertical spacing of C-channels (S_v), and horizontal spacing of C-channels (S_h). Followed discussions were also carried out on effects of these parameters on axial compressive behaviours of SCSSCW-ECs. Including experimental studies, analytical models were also developed to predict the ultimate compressive resistance of SCSSCW-ECs, and their accuracies were validated by 11 test results in this paper.

2 Compressive tests on SCSSCW-ECs

2.1 Details of SCSSCW-ECs

Figure 2 shows the representative SCSSCW-ECs, which comprises two external steel faceplates, a concrete core, C-channels, and bolts. The fabrication procedures of SCSSCW-ECs include welding the C-channels to faceplates with reserved holes, assembling two faceplates and screwing in bolts from external side of specimen, and concrete casting. More details of this novel SCSSCW have been reported by Yan et al. [28-29]. Seven SCSSCW-ECs were prepared in this study, and Fig. 3 shows the preparation of these specimens. It can be found that the developed SCSSCW-ECs only require preparing mould at one open side surface [see Fig. 3(b)], and reduce the site labour force for casting [see Fig. 3(c)]. Furthermore, four tests in Ref. [28] were also included in this study for discussion and analysis purposes. Thus, there are totally 11 tests available for this study. Fig. 4 shows the geometry of SCSSCWs. It can be found that all the specimens are in the same dimensions with the height, width, and depth (concrete core) of 660, 600, and 120 mm, respectively. The thickness of faceplate (t_s) and layout of inside C-channels varies with different specimens. Two SCSSCW-ECs, namely DW1-1 and DW1-2 were prepared with the controlling parameters, i.e., t_s=3.0 mm, C50 normal weight concrete (f_c=54.4 MPa), S_v=90 mm, S_h=140 mm, and installed C-channels with horizontal-web. SCSSCW DW2 [28] was prepared with the same parameters as DW1 except the direction of C-channels inside the steel skeleton, i.e., C-channels installed with vertical-web (V-web). SCSSCWs DW1, DW3 [28], and DW4 were designed with the same parameters except different

t_s values of 3.0, 4.5, and 6.0 mm. Two identical specimens DW5-1 and DW5-2 were prepared with lower strength concrete core (f_c=45.6 MPa) compared with that of DW1. SCSSCWs DW1, DW6 [28], and DW7 were designed with different vertical spacing of C-channels (S_v) of 90, 130, and 170 mm, respectively. Meanwhile, DW1, DW8 [28], and DW9 were designed with different horizontal spacing of C-channels (S_h) of 90, 200, and 290 mm, respectively. Table 1 summarizes more details of DW1~9.

2.2 Materials

The SCSSCW-ECs adopted 3.0, 4.5, and 6.0 mm- thick Q235B mild steel faceplates for their fabrications. Q235B C-channel in height of 120 mm was selected as the shear connector for all SCSSCW-ECs, and their geometric details can be found in Fig. 2. The mechanical properties of these steel faceplates and C-channels were obtained from standard tension tests on coupons cut from them in accordance with Chinese code GB/T228.1 [30]. Finally, the obtained stress-strain curves of three kinds of faceplates and C-channels are shown in Fig. 5. The details of mechanical properties, e.g., yield and ultimate strength, are given in Table 1. The core of SCSSCW-ECs adopts C40 and C50 normal weight concrete (NWC). Cubes with width of 100 mm and prisms measuring 100×100×300 mm^3 were tested to obtain compressive strengths of NWC. Table 1 lists more details on mechanical properties of NWC and mild steel. M8.8 grade type of bolts (measuring 14 mm × 40 mm in diameter × height) were used in SCSSCW, and their yield strengths are 640MPa. With the parameter analysis of the tolerance, a distance of 0.5-1.5mm between hole and bolt has little influence on shear strength of enhanced C-channel connectors, meanwhile the ductility of the connectors

and convenience of fabrication have been greatly improved. Yan et al. [29] discussed the mechanical property of ECs in detail.

2.3 Setup and measurements

All the axial compression tests on SCSSCW-ECs were performed in Concrete Structural Laboratory, Tianjin University by a SHIDAI SHIJING testing machine with its compression capacity of 1500 tons. The compression-testing machine (YAW-15000F) is made in Shandong, China and the measurement errors of force and displacement are less than 1%. Fig. 6 shows the setup of these performed axial compression tests. The specimen was put on the rigid bottom-holding frame. During testing, the quasi-static displacement loading in a rate of 0.05 mm/min was applied to the top end plate of SCSSCW-ECs by an actuator. In addition, the reaction forces actting on the specimen were measured by a load cell underneath the bottom end. Linear varying displacement transducers (LVDTs) were used for the measurements of shortenings of SCSSCW-ECs during the testing. For bottom and top end plates of each SCSSCW-ECs, six LVDTs were installed on each of them to measure their displacements as shown in Fig. 6. Finally, their average values will be used for the determination of shortenings of SCSSCW-ECs. To measure the strains developed in faceplates, linear strain gauges were also installed on their external surfaces, and Fig. 6 shows their positions. During the tests, the loading rate and different kinds of readings were controlled and recorded on a PC controlling system.

3 Test results and discussions

3.1 Failure modes

Figure 7 plots the sequences of observed failure modes and cracks in the concrete from two open side surfaces of specimens. It shows that the common failure modes occurred to these two external steel faceplates are local buckling whilst the typical failure modes occurred to the concrete core are crushing and splitting. However, there are still existing differences among the local buckling occurred to specimens with different spacing of C-channels. Thus, specimens DW1-1, DW2, DW4, DW5, DW7, and DW9 were selected for the illustration on their failure modes for each investigated parameters.

Fig. 7(a) illustrates the failure modes and their occurrence sequences in faceplate and concrete core for specimen DW1-1 during the loading process. As the reaction force (P) achieved 1050 kN, minor local buckling was observed at position (1) as shown in Fig. 7(a). As the P value increased to 2855 kN, separation of the faceplate and concrete between two rows of connectors was observed at position (1). After that, as P equals to 3845 kN, separations of faceplate from concrete core between two rows of faceplates at positions (2) and (3) were observed; meanwhile, concrete crushing (CS) was observed at position I. As P increased to 4200 kN, faceplate at position (4) was observed separating from the concrete core. At the ultimate load of about 4800 kN, the severe local buckling was observed in steel faceplates, and the whole strip of faceplates at position (4) and (6) between two rows of connectors all buckled. Meanwhile, concrete crushing occurred at the bottom portion of specimens. After that,

during the loading recession, as the load decreased to about 3000 kN, concrete splitting at position II was observed.

Fig. 7(b) depicts failure modes as well as their sequences of specimen DW2. As the load *P* increased to about 600 kN, steel faceplates at position (1) and (2) exhibited slight local buckling. As *P* increased to about 1500 kN, concrete splitting at position I was observed. After that, as *P* increased to about 1900 kN, steel faceplates at positions (3) and (4) exhibit outward local buckling. With the increase of *P* to about 3500 kN, concrete at position III exhibited crushing mode, and local buckling of faceplates at position (5) took place. At the ultimate load point, the whole strip all locally buckled between two rows of connectors at position (4) and (6); meanwhile, the concrete core failed in crushing.

Fig. 7(c) plots the failure modes of DW4. After testing as the load *P* increased to about 4500 kN, vertical cracks at position I and II in the concrete core took place. As *P* increased to 4781 kN, separation of steel faceplate from the concrete core at position (1) took place, and vertical cracks took place in the concrete core at position III; meanwhile, the concrete at position I were peeled off. As *P* increased to the ultimate load of 5971 kN, outward buckling occurred the steel-faceplate strip at position (2), and slight separation of faceplate from concrete core was observed at position (3); meanwhile, the obvious local buckling occurred in faceplates at position (1) and the whole strip of faceplate at position (1) all buckled along the width of specimen. After that during the recession of loading, as *P* decreased to 3750 kN, the steel faceplates at positions (2) and (3) exhibited severe local buckling.

Fig. 7(d) exhibits failure modes of DW5-1. During the loading, as the *P* increased to 1813, 2220, and 2542 kN, slight local buckling occurred to faceplates at position (1), (2) and (3), respectively. As *P* increased to 2931 kN, cracking was observed at position I in the concrete core; meanwhile, slight separation of the faceplate from the concrete core was observed at position (4). As *P* increased to 3133 kN, buckling in local region (5) of faceplate took place; meanwhile, the local buckling areas in positions (2) and (4) were enlarged. At the ultimate load of 3991 kN, the local buckling occurred in positions (6)~(8), and the concrete crushing became more seriously at the foot of specimen. In addition, the whole strip of faceplate along the width almost buckled between two rows of connectors at position (8).

Fig. 7(e) exhibits failure modes of DW7. During the loading process, as *P* increased to 1444 kN, slight local buckling was observed at position (1) of the steel faceplates and slight separation between the concrete and faceplate was observed at position (2). As *P* increased to 1800 kN, local buckling at position (3) was observed; slight separation of faceplate from the concrete core was observed at position (4); diagonal splitting crack was observed at position I; and local buckling at position became more serious. As *P* increased to 2485 kN, local buckling in the faceplate was observed at position (5), and cracks were observed in the concrete at positon II. At loading level of 3810 kN, local buckling was observed at position (6) in the faceplate. Finally, at ultimate load of 4227 kN, concrete crushing took place and local buckling propagates through the whole strip of faceplate between two rows of C-channels at positions (1) and (4).

Fig. 7(g) exhibits failure modes of DW9. As the load increased to 700 kN, slight local buckling took place at positions (1) and (2) of the faceplate. At loading level of 1050 kN, minor local buckling occurred to faceplate at position (3). As *P* increased to 1670 kN, the local buckling of faceplate at positions (1) and (4) connected and gradually merged; meanwhile, minor local buckling occurred to faceplate at position (5). As *P* increased to 2880 kN, the local buckling regions at position (5) and (6) connect and merge, which means the strip along the width of the specimen all buckled. As *P* increased to 3230 kN, splitting occurred to the concrete core at position I. Finally, at the ultimate load of 4225 kN, major local buckling occurred to the faceplate at position (7), concrete splitting occurred to position III and crushing was observed at position I and II in the concrete core.

3.2 Axial load-shortening and load-strain behaviours

Figure 8 plots the axial load-shortening (*P-Δ*) curves of SCSSCW-ECs. Fig. 8(e) plots summarized general *P-Δ* curves of SCSSCW-ECs under axial compression. Fig. 9 plots the representative load-strain curves of faceplates. They show that SCSSCW-ECs exhibit a three-stage working mechanism subjected to axial compression that include linear, nonlinear, and post-peak recession working stage. The first linear working stage starts from the loading and ends at the occurrences of minor local buckling in the steel faceplates at several locations (e.g., DW1, DW2, DW6, and DW7) or yielding of the external steel faceplates at some locations, e.g., DW3, DW4, DW5, and DW8. The elastic limit load (P_e) equals to about 60%~80% of the ultimate load. Though minor local buckling occurs at some locations in the steel

faceplates during the elastic working stage in most of the specimens, e.g., DW1-1, DW2, DW4~9, the load-shortening curves show that their elastic stiffness was only slightly affected. This is because that the minor local buckling only slightly affects the stiffness of faceplates, but the elastic stiffness of concrete core was not affected. This can be also reflected in linear behaviour of load-strain curves of steel faceplates as shown in Fig. 9. In the second nonlinear working stage, the SCSSCW exhibits nonlinear load versus shortening behaviours that were mainly produced by nonlinear mechanical properties of the concrete and faceplates, and developments of local buckling of faceplates. For specimens DW2, DW6, and DW7, their load-strain curves show that elastic local buckling occurs to their steel faceplates at the nonlinear working stages. Moreover, concrete splitting and nonlinear mechanical properties of concrete core mainly contribute to their nonlinear load-shortening behaviours. Finally, at the finishing point of the second stage, major local buckling and concrete crushing occurred to them. For the rest specimens (e.g., DW1, DW3~5, and DW8), it can be found that the load-strain curves all exceed their yielding strains that means plastic buckling of faceplate at stage II. Thus, the nonlinear behaviour of these specimens at the second working stage was contributed by the nonlinearities of both steel faceplates and concrete core, concrete splitting/crushing, and plastic buckling of faceplates. Finally, at the ultimate loading point, concrete crushing and major local buckling occurred. After that, in the third working stage, severe concrete crushing or splitting (see Fig. 7) took place in the concrete and major local buckling of faceplates occurred in more locations. Specimens with lower strength [e.g., specimen DW5 in Fig. 8(c)]

exhibit more flat recession branches in the load-shortening curves. Meanwhile, the specimens with larger spacing of C-channels, e.g., specimens DW6 and DW7 in Fig. 8(d) exhibit sharper drops in their recession branches of load-shortening curves.

3.3 Elastic stiffness, ultimate compressive resistance, and ductility index

The ultimate compressive resistance (P_u) of SCSSCW-ECs could be observed form the load-shortening and load-strain curves in Fig. 8~9. The elastic stiffness (K_e) of SCSSCW-ECs are determined following the method in Ref. [17], i.e., the 30% ultimate load ($P_{0.3}$) to its shortening ($\Delta_{0.3}$) ratio as follows;

$$K_e = \frac{P_{0.3}}{\Delta_{0.3}} \tag{1}$$

The ductility index (*DI*) proposed in Ref. [10] was adopted to describe the ductility of SCSSCW-ECs as the following;

$$DI = \frac{\Delta_{85\%}}{\Delta_u} \tag{2}$$

where, $\Delta_{85\%}$ is shortening at 85%P_u in the recession branch of load-shortening curves; Δ_u is the shortening at P_u.

Finally, these determined K_e, P_u, Δ_u and *DI* ratios for SCSSCW-ECs are listed in Table 1.

3.4 Discussions

The effects of studied parameters on compressive behaviour of SCSSCW-ECs are herein discussed and analysed.

3.4.1 Effect of layout of C-channel

The C-channels in the developed SCSSCW-ECs could be installed with its web parallel or perpendicular to the axial loading direction, and these two layout of C-channels were named as horizontal web (H-web) and vertical web (V-web), respectively. The layout of H-web and V-web are detailed plotted in Fig. 4. Fig. 8(a) depicts the effect of layout of C-channels on load-shortening curves of SCSSCW-ECs. Fig. 10(a) and (b) depicts influences of layout of C-channel on strength (K_e, P_u) and ductility (Δ_u and *DI* ratio) indexes, respectively. Fig. 8(a) exhibits that the direction of C-channel does not affect the elastic behaviour, but affects the nonlinear and recession working stages of load-shortening curves of SCSSCW-ECs. As reflected in Fig. 10(a) and (b), the SCSSCW-EC with H-web exhibits 7%, 4%, 1%, and 9% higher in P_u, K_e, Δ_u and *DI* ratio than those with V-web. The influence of layout of C-channel is quite limited on its elastic stiffness and Δ_u. However, as reflected in Fig. 4, the quantity of ECs in DW1 is even less than that in DW2. Moreover, the slenderness ratios for the faceplates in DW1 and DW2 are also close, which means the layout of C-channel does not affect the compressive resistance of faceplates. Thus, the concrete core mainly causes these differences in strength and ductility indexes. This can be explained by that the vertical web of C-channels paralleling to the loading direction results in stress concentration at the vertical web toe to the concrete, which will split the concrete core [see Fig. 7(b)]. Thus, the web of C-channels were recommended to be installed horizontally, i.e., the perpendicular direction to the axial compression axis.

3.4.2 Effect of faceplate thickness (t_s)

The influences of t_s on load-shortening behaviours of SCSSCWs are plotted in Fig. 8(b) whilst Fig. 10(c) and (d) shows effects of t_s on strength and ductility of SCSSCWs. These figures exhibit that increasing the faceplate thickness generally improves the load-shortening behaviours of SCSSCWs under axial compression. With the increase of t_s from 2.9 to 4.8 and 5.6 mm the P_u is improved by 29% and 28%, respectively; meanwhile, the increments in K_e are 11% and 24%, respectively. This can be easily understood that increasing t_s leads to increased steel content and equivalent depth for the cross section of SCSSCW-ECs. These increments in the cross section improved both elastic stiffness and ultimate compressive strength of SCSSCW-ECs. Moreover, the slenderness ratio ($\lambda=S_{va}/t_s$) of the faceplate under axial compression is reduced from 31.6 to 18.8 and 16.1 as t_s increases from 2.9 to 4.8 and 5.6 mm, which finally resulted in improved compressive resistance of faceplates. Increasing the faceplate thickness from 2.9 to 4.8 mm improves the ductility of SCSSCWs, which shows 12% increase in the *DI* ratio. However, the test results also show that with the increase of t_s from 4.8 to 5.6 mm, both P_u and *DI* ratios were not improved except the 13% increase in the K_e value. The reason for the limited influences on both P_u and *DI* ratio is that the earlier crushing of concrete core occurred to DW4 with t_s=5.6 mm than DW3 with t_s=4.8 mm. This can be clearly found in load-strain curve of DW4 in Fig. 9(e) that there is an obvious changing point at about 4000 kN, which is caused by local crushing of concrete core. This also can explain that with the increase of t_s from 4.8 to 5.6 mm the *DI* ratio is not affected due to the early local crushing of concrete core.

3.4.3 Effect of concrete core strength (f_c)

Fig. 8(c) depicts the effect of f_c on *P-Δ* behaviours of SCSSCW-ECs. The influences of f_c on K_e, P_u, Δ_u and *DI* ratios of SCSSCW-ECs are shown in Fig. 10(c)~(d). These figures exhibit that increasing the strength of concrete core generally improves the K_e and P_u of SCDSSCW-ECs, but compromises its ductility. With the increase of f_c from 45.6 to 54.4 MPa, this 19% increase in f_c results in 18% and 14% increments in P_u and K_e of SCSSCWs, respectively; however, the *DI* ratio of SCSSCWs is reduced by 24%. The reason of improvements on P_u and K_e of SCSSCWs through using higher-grade concrete is that higher strength concrete provides both higher modulus and ultimate compressive strength. However, higher grade concrete tends to be more brittle, which reduces the ductility of SCSSCWs.

3.4.4 Effect of vertical spacing of ECs (S_v)

Fig. 8(d) plots the influence of S_v on *P-Δ* behaviours of SCSSCW-ECs. Fig. 10(g) and (h) exhibits influences of S_v on strength and ductility indexes of SCSSCW-ECs. They support observations as the following;

(1) With the increase of S_v from 90 to 130 and 170 mm, the P_u value of SCSSCW-ECs is reduced by 10% and 10%, respectively; meanwhile, the K_e value of SCSSCW-ECs is reduced by only 2%, and 3%, respectively. This reflects that the increasing S_v value reduces the ultimate compressive resistance of SCSSCW-ECs, but has quite ignorable influence on its elastic stiffness. This is because that the increasing the S_v value from 90 to 130 and 170 mm increases the

λ value of faceplate from 31.6 to 44.8 and 55.0, which reduces the compressive resistance of faceplates as well as the P_u value of SCSSCW. However, during the elastic working stage of SCSSCW, this increasing S_v value does not affect the cross-sectional stiffness. Thus, this explains the marginal influence of increasing S_v value on K_e of SCSSCW-ECs.

(2) As the S_v value increases from 90 to 130 and 170 mm, the *DI* ratio of SCSSCW-ECs is reduced by 11% and 7%, respectively. The increasing S_v value exhibits negative influence on the ductility of SCSSCW-ECs. This is because as the S_v value increases, the increasing slenderness ratio of the faceplate would change the failure mode of faceplates from plastic to elastic buckling, which can be reflected in Fig. 9. This early elastic buckling of faceplate tends to reduce the ductility of SCSSCW-ECs.

Thus, in the design of SCSSCW-ECs, the vertical spacing of C-channel requires careful consideration.

3.4.5 Effect of average horizontal spacing of ECs (S_h)

Fig. 8(e) plots the influence of S_h on *P-Δ* cures of SCSSCW-ECs. Fig. 10(i) and (j) exhibits influences of S_h on strength and ductility indexes of SCSSCW-ECs. These figures show that though specimens S1, S8, and S9 were designed with the same vertical spacing of C-channels of 90 mm, as the S_h value increases from 115 to 175 and 265 mm, the P_u of SCSSCW-ECs is reduced by 5% and 8%, respectively; however, the K_e of SCSSCW-ECs is almost unchanged with slight differences less

than 1.0%. This is because that as the S_h increases the restraints of the horizontal strip of faceplate on buckling of the vertical strip of faceplate tend to decrease, which could not effectively restrain the local buckling of faceplates between two neighbouring rows of C-channels. This can be clearly found in Fig. 7(g) and (f) that the vertical strip locally buckles skipping the neighbouring rows of C-channels, i.e., the buckling length of faceplates is between the first and third row of C-channels. This is because that under compression, the buckling of steel faceplates were restrained by the C-channels and externally connected bolts at points. Thus, as the horizontal spacing of C-channels increases, the restraints on the middle strip of faceplate are weaken and local buckling length of middle strip of faceplate tends to be beyond one times S_v, which reduces the compressive strength of faceplates. Thus, the influence of S_h needs to be considered in the design of compressive resistance of SCSSCW-ECs.

4 Analysis on ultimate compressive resistance of SCSSCW-ECs

4.1 Theoretical models

The axial compressive resistance of SCSSCW-ECs (N_T) can be determined as the following;

$$N_T = N_c + N_s \tag{3}$$

where, N_c is concrete-core compressive resistance; N_s is the compressive resistance of faceplates.

Since C-channels in the cross section tend to confine the concrete between the two flanges, the compressive strength of concrete in different regions of the cross section

tends to be different as illustrated in Fig. 11. Thus, the average compressive stress $\bar{\sigma}_c$ is used to determine N_c value of SCSSCW-ECs. The N_c value in SCSSCW-ECs is determined as the following [28];

$$N_c = \bar{\sigma}_c A_c \tag{4}$$

$$\bar{\sigma}_c = \frac{L_c}{S_h}\sigma_{cc} + \frac{S_h - L_c}{S_h} f_c \tag{5}$$

$$\sigma_{cc} = \frac{\left(1+2\alpha_s^2\right)\sigma_{cf} + 2(1-\alpha_s)\alpha_s f_c + \sqrt{\begin{matrix}\left[\left(1+2\alpha_s^2\right)\sigma_{cf} + 2(1-\alpha_s)\alpha_s f_c\right]^2 - \\ 4(1-\alpha_s^2)\left\{\sigma_{cf}^2 - \left[\left(1-\alpha_s\right) f_c + \alpha_s\sigma_{cf}\right]^2\right\}\end{matrix}}}{2(1-\alpha_s^2)} \tag{6}$$

$$\sigma_{cf} = \frac{T_C}{S_{va}S_{ha}} = \min\begin{Bmatrix} T_{cs} = A_{sc}\sigma_{uc} \\ T_{cb} = A_{sb}\sigma_{ub} \end{Bmatrix} \Big/ S_{va}S_{ha} \tag{7}$$

where, σ_{cc} is the compressive stress of concrete confined by faceplates; f_c is cylindrical compressive strength of concrete; A_c is the sectional size of concrete core; L_c is the length of C-channel flange; S_h is horizontal spacing of connectors; σ_{cf} is the confining stress on concrete core by steel skeleton; α_s is the coefficient, and herein equals to 0.19; T_c is tensile resistance of ECs; S_{va} is the average vertical spacing of ECs; S_{ha} is the average horizontal spacing of ECs; T_{cs} and T_{cb} are the tensile resistance of C-channel web and anchoring bolt; σ_{uc} and σ_{ub} are the tensile strength of C-channel web and anchoring bolt; A_{sc} is the area for web cross section in C-channel; A_{sb} is cross-sectional area of externally connected bolt.

Considering the influences of different buckling length of faceplates in different regions as pointed in section 3.4.5, based on the experimental observations, Fig. 12

proposes a method to differentiate the faceplates into different vertical strips, i.e., strip A~C. According to the experimental measurements in Fig. 12, strips A, B, and C are the vertical strip of faceplate locating within $\pm 1.0\ L_c$ of a vertical column of C-channels (L_c denotes the length of C-channel flange), the rest strip between two columns of C-channels, and edge strip, which are highlighted in Fig. 12. Thus, different buckling lengths for these strips A~C can be adopted for the determination of their compressive resistances. As pointed in Fig. 13, outward buckling takes place and the buckling length of different strips in the faceplate varies with their positions. Thus, the determinations on N_s of faceplates in SCSSCW-ECs are as follows;

$$N_s = \sum_{i=1}^{a} \sigma_{cr,i} A_{s,Ai} t_s + \sum_{j=1}^{b} \sigma_{cr,j} B_{s,Bj} t_s + \sum_{k=1}^{c} \sigma_{cr,k} C_{s,Ck} t_s \tag{8}$$

$$\sigma_{cr,i} = \min\left(\frac{\pi^2 E_s}{12K^2 \left(\eta_i S_v / t_s\right)^2}, f_{ys} \right) \tag{9}$$

$$\eta_i = \begin{cases} 1.0 & \text{for strip A faceplate} \\ S_h / S_v & \text{for strip B,C faceplate, and } S_h \geq S_v \end{cases} \tag{10}$$

where, $\sigma_{cr,i}$ denotes critical buckling stress of different strip of faceplate as shown in Fig. 12; $A_{s,Ai}$, $B_{s,Bj}$, and $C_{s,Ck}$ denote width of the A~C strip of faceplates in Fig. 13; *a*, *b*, and *c* denote number of A, B, and C type of strips in faceplates as shown in Fig. 13, respectively; *K* is the boundary condition coefficient, and herein equals to 0.825; η_i is the buckling length coefficient for different faceplate strip; S_h and S_v denote horizontal and vertical spacing of ECs, respectively; E_s is the elastic modulus; f_{ys} denotes yield strength; t_s is the thickness of steel faceplate.

4.2 Code provisions

Following AISC360-10 [31], the ultimate compressive resistance for SCSSCW-ECs (N_{uA}) can be determined as follows;

$$N_{uA} = \begin{cases} 0.658^{N_0/N_{cr}} N_0, & N_0 \le 2.25 N_{cr} \\ 0.877 N_{cr}, & N_0 > 2.25 N_{cr} \end{cases} \tag{11}$$

$$\begin{aligned} N_0 &= f_y A_s + 0.85 f_c A_c \\ N_{cr} &= \frac{\pi^2}{KL} EI_{eff} \end{aligned} \tag{12}$$

where, N_0 is nominal compressive strength of zero length, axially loaded composite member; N_{cr} is the elastic critical buckling load; $EI_{eff} = E_s I_s + \gamma E_c I_c$ for cross section for SCSSCW-ECs; $\gamma = 0.1 + 2\frac{A_s}{A_s + A_c} \le 0.3$; L is laterally unbraced length of the member; f_y is the yield strength of steel faceplate; f_c is cylindrical compressive strength of concrete; A_s and A_c are the cross-sectional area of steel and concrete.

According to Eurocode 4 [32], the ultimate compressive resistance of SCSSCW-ECs, N_E, is determined as the following;

$$N_E = \chi N_0 \tag{13}$$

$$N_0 = f_y A_s + 0.85 f_c A_c \tag{14}$$

$$\chi = \frac{1}{\Phi + \sqrt{\Phi^2 - \lambda^2}} \le 1.0 \tag{15}$$

$$\Phi = 0.5[1 + \alpha(\lambda - 0.2) + \lambda^2] \tag{16}$$

$$\lambda = \sqrt{\frac{N_0}{N_{cr}}} \tag{17}$$

where, χ is the reduction factor for flexural buckling; N_0 is the plastic resistance of the composite section to compressive normal force; f_y is the yield strength of steel faceplate; f_c is cylindrical compressive strength of concrete; A_s and A_c are the cross-sectional area of steel and concrete; λ is the relative slenderness; N_{cr} denotes the elastic critical buckling force that can be determined by the effective flexural stiffness $(EI)_{eff} = E_s I_s + K_e E_c I_c$; K_e=0.6 is a coefficient.

In Chinese code CECS [33], the determination on compressive resistance of SCSSCW-ECs follows the specifications as the following;

$$N_{CN} = \varphi N_0 \tag{18}$$

$$N_0 = f_y A_s + f_c A_c \tag{19}$$

$$\varphi = \begin{cases} 1 - 0.65\lambda_0^2 & \text{for } \lambda_0 \le 0.215 \\ \dfrac{1}{2\lambda_0^2}[(0.965 + 0.3\lambda_0 + \lambda_0^2) & \\ -\sqrt{(0.965 + 0.3\lambda_0 + \lambda_0^2)^2 - 4\lambda_0^2}] & \text{for } \lambda_0 > 0.215 \end{cases} \tag{20}$$

$$\lambda_0 = \frac{l_0}{\pi\sqrt{\dfrac{I_s + I_c E_c / E_s}{A_s + A_c f_c / f_y}}}\sqrt{\frac{f_y}{E_s}} \tag{21}$$

where, φ is the stability coefficient; N_0 is the plastic resistance of the composite section; f_y is the yield strength of steel faceplate; f_c is cylindrical compressive strength of concrete; A_s and A_c are the cross-sectional area of steel and concrete; E_s and E_c are the elastic modulus of steel and concrete; I_s and I_c are the inertia moment of steel and concrete; λ_0 is the generalized slenderness ratio.

4.3 Validations

Table 2 compares predicted ultimate compressive resistances of SCSSCW-ECs by the developed theoretical model (TM), AISC360 [31], Eurocode 4 [32], and CECS [33] with the experimental results. Fig. 14 compares the scatters of test-to-prediction ratios by these four methods. These figure and table show that the TM and CECS offer the most accurate predictions to test results with average prediction errors of 3% and 2%, respectively. Eurocode 4 provides the second most conservative estimations on the ultimate compressive resistance of SCSSCW-ECs with an average prediction error of 6%. AISC360 [31] offers the most conservative predictions on P_u of SCSSCW-ECs with an average prediction error of 11%. However, the developed TM offers the smallest coefficient of variation (COV) of 0.05 compared with 0.09 for the three codes, i.e., AISC [31], Eurocode 4 [32], and CECS [33]. Thus, considering both average prediction errors and COV, TM offers the most accurate estimations on P_u of SCSSCW-ECs. The prediction errors of the developed TM may be from the ignorance of the geometric imperfection of the specimen and overestimation on the compressive strength of concrete core.

However, the developed models are only validated by the reported 11 test results. More extensive validations are still required.

5 Conclusions

This paper firstly proposed a new type of SCSSCWs with novel enhanced C-channels (ECs). Then, this paper studied compressive behaviours of this novel SCSSCW-ECs

and their influencing parameters through full-scale tests. Followed, theoretical models were proposed to estimate P_u of SCSSCW-ECs. In addition, the code equations were also used to predict the P_u of SCSSCW-ECs. From these studies, the following conclusions are drawn;

(1) Failure modes occurred to SCSSCW-ECs under axial compression include concrete crushing and local buckling of steel faceplates. The horizontal spacing of ECs influences the vertical buckling length of faceplates as well as compression behaviour of SCSSCW-ECs.

(2) Axial load-shortening curves of SCSSCW-ECs exhibited a three-stage working mechanism that include linear, nonlinear, and post-peak recession working stage. The local buckling of faceplates mainly causes the shifting from linear to nonlinear stage. Local buckling of faceplates and nonlinearities of both faceplate and concrete mainly influenced the nonlinear behaviours of SCSSCW-ECs. At the ultimate load, concrete crushing and local buckling of faceplate occurred to SCSSCW-ECs.

(3) SCSSCW-ECs with H-web exhibited about 7% larger P_u value than that with V-web due to splitting in concrete core induced by the V-web due to avoiding the stress concentration at the web position of C-channel. The C-channels were recommended to be installed with their webs perpendicular to the axial compression.

(4) Increasing t_s of faceplate generally improves the load-shortening behaviours of SCSSCWs under axial compression. Increasing t_s from 2.9 to 5.6 mm improved

the P_u and K_e of SCSSCW-ECs by 28% and 24%, respectively.

(5) With the increase of f_c from 45.6 to 54.4 MPa, 20% increase in f_c results in 18% and 14% increments in P_u and K_e of SCSSCWs, respectively, but reduced its ductility by 24%.

(6) As the S_v value increases from 90 to 130 and 170 mm, the P_u and ductility ratio of SCSSCW-ECs are reduced by about 10%, but its K_e value is almost unaffected. The increasing S_v value only compromises its second nonlinear working stage of SCSSCW-ECs, but does not affect its first linear working stage.

(7) As the horizontal spacing of S_h value increases from 115 to 265 mm, the ultimate compressive resistance of SCSSCW-ECs is reduced by about 10% through affect the buckling length of faceplates.

(8) Developed theoretical models offer the most accurate predictions on P_u of SCSSCW-ECs with an average 3% prediction error and a low COV of 0.05. The AISC offers the most conservative predictions with an average 11% prediction error whilst EC4 offers the second most conservative prediction with an average error of 6%. The developed theoretical models are recommended for estimations on P_u of SCSSCW-ECs. However, further validations are still required due to the limited validations against only 11 test results.

ACKNOWLEDGMENT

The authors would like to acknowledge the research grant 51608358 received from National Natural Science Foundation of China and Peiyang Scholar Foundation (grant no. 2019XRX-0026) under Reserved Academic Program from Tianjin University for

the works reported herein. The authors gratefully express their gratitude for the financial supports.

References

[1] X. Ji, F. Jiang, J. Qian, Seismic behavior of steel tube–double steel plate–concrete composite walls: Experimental tests, J. Constr. Steel Res. 86 (2013) 17–30.

[2] X. Ji, X. Cheng, X. Jia, A.H. Varma, Cyclic in-plane shear behavior of double-skin composite walls in high-rise buildings. ASCE, J. Struct. Eng. 143 (6) (2017) 04017025.

[3] J.G. Nie, H.S. Hu, J.S. Fan, M.X. Tao, S.Y. Li, F.J. Liu, Experimental study on seismic behaviour of highstrength concrete filled double-steel-plate composite walls, J. Constr. Steel Res. 88(2013) 206-219.

[4] K. Zhang, A.H. Varma, S.R. Malushte, S. Gallocher, Effect of shear connectors on local buckling and composite action insteel concrete composite walls, Nucl. Eng. Des. 269(2014) 231– 239.

[5] Y.Z. Lin, J.C. Yan, Z.G. Cao, X.Z. Zeng, F. Fan, C.Y. Zou, Ultimate strength behaviour of S-UHPC-S and SCS sandwich beams under shear loads, J. Constr. Steel Res. 149 (2018) 195-206.

[6] W.J. Zhang, A. Koizumi, Behavior of composite segment for shield tunnel, Tunn. Undergr. Sp. Tech. 25 (4) (2010) 325-332.

[7] M. Lin, W. Lin, Q. Wang, X. Wang, The deployable element, a new closure joint construction method for immersed tunnel, Tunn. Undergr. Sp. Tech. 80 (2018) 290-300.

[8] C. Yan, Y.H. Wang, X.M. Zhai, L.Z. Meng, H.Y. Zhou, Experimental study on curved steel-concrete-steel sandwich shells under concentrated load by a hemi-spherical head, Thin-Walled Struct. 137 (2019) 117-128.

[9] Y.H. Wang, X.M. Zhai, S.C. Lee, W. Wang, Responses of curved steel-concrete-steel sandwich shells subjected to blast loading, Thin-Walled Struct. 108 (2016) 185-192.

[10] J.B. Yan, Z. Wang, Y.B. Luo, T. Wang, Compressive behaviours of novel SCS sandwich composite walls with normal weight concrete, Thin-Walled Struct. 141 (2019) 119-132.

[11] J.B. Yan, Z. Wang, J. Xie, Compressive behaviours of double skin composite walls at low temperatures relevant to the Arctic environment, Thin-Walled Struct. 140 (2019) 294-303.

[12] J.B. Yan, Z. Wang, T. Wang, Compressive behaviours of novel steel-concrete-steel sandwich walls at low temperatures, Constr. Build. Mater. 207 (2019) 108-121.

[13] A. Remennikov, E.C.J. Gan, T. Ngo, M.D. Netherton, The development and ballistic performance of protective steel concrete composite barriers against hypervelocity impacts by explosively formed projectiles, Compos. Struct. 207

(2019) 625-644.
[14] A. Ghabussi, J.A. Marnani, M.S. Rohanimanesh. Improving seismic performance of portal frame structures with steel curved dampers. Structures 24 (2020) 27-40.
[15] M. Safarpour, A. Ghabussi, F. Ebrahimi, M. Habibi, H. Safarpour. Frequency characteristics of FG-GPLRC viscoelastic thick annular plate with the aid of GDQM. Thin-Walled Struct. 150 (2020) 106683.
[16] B.J. Choi, C.K. Kang, H.Y. Park, Strength and behavior of steel plate–concrete wall structures using ordinary and eco-oriented cement concrete under axial compression, Thin-Walled Struct. 84 (2014) 313-324.
[17] B.J. Choi, H.S. Han, An experiment on compressive profile of the unstiffened steel plate-concrete structures under compression loading, Steel Compos. Struct. 9(6) (2009) 519-534.
[18] A.H. Varma, S.R. Malushte, K.C. Sener, Z. Lai, Steel-plate composite (SC) walls for safety related nuclear facilities: Design for in-plane forces and out-of-plane moments, Nucl. Eng. Des. 269 (2014) 240-249.
[19] J.B. Yan, Z.X. Li, T. Wang, Seismic behaviour of double skin composite shear walls with overlapped headed studs, Constr. Build. Mater. 191(2018) 590-607.
[20] M. Xie, J.C. Chapman, Development in Sandwich Construction, J. Constr. Steel Res. 62(11) (2006) 1123-1133.
[21] M. Xie, N. Foundoukos, J.C. Chapman, Static tests on Steel–Concrete–Steel sandwich beams, J. Constr. Steel. Res. 63(6) (2007) 735-750.
[22] M. Xie, N. Foundoukos, J.C. Chapman, Experimental and numerical investigation on the shear behaviour of friction-welded bar–plate connections embedded in concrete, J. Constr. Steel Res. 61 (2004) 625–649.
[23] J.Y.R. Liew, K.M.A. Sohel, C.G. Koh, Impact Tests on Steel–Concrete–Steel Sandwich Beams with Lightweight Concrete Core, Eng. Struct. 31(9) (2009) 2045-2059.
[24] J.B. Yan, Y.Y. Yan, T. Wang, Z.X. Li, Seismic behaviours of SCS sandwich shear walls using J-hook connectors, Thin-Walled Struct. 144(2019) 106308.
[25] J.B. Yan, Y.Y. Yan, T. Wang. Seismic behaviours of novel SCS sandwich shear walls with CFST boundary columns, J. Constr. Steel Res. 164(2020) 105760.
[26] Y. Qin, Y.W. Li, Y.S. Su, X.Z. Lan, Y.D. Wu, X.Y. Wang, Compressive behavior of profiled double skin composite wall, Steel Compos. Struct. 30(5) (2019) 405-416.
[27] Y.Qin, Y.W. Li, X.Z. Lan, Y.S. Su, X.Y. Wang, Y.D. Wu, Structural behavior of the stiffened double-skin profiled composite walls under compression, Steel Compos. Struct. 31(1) (2019) 1-12.
[28] J.B. Yan, A.Z. Chen, T. Wang, Developments of double skin composite walls using novel enhanced C-channel connectors, Steel Compos. Struct. 33(6) (2019) 877-889.

[29] J.B. Yan, H.T. Hu, T. Wang, Shear behaviour of novel enhanced C-channel connectors in steel-concrete-steel sandwich composite structures. J. Constr. Steel Res. 166 (2020) 105903.
[30] GB/T228.1—2010, Metallic Materials: Tensile testing, China Planning Press, Beijing, 2010 (in Chinese).
[31] AISC 360–16, Specification for Structural Steel Buildings, American Institute of Steel Construction, Chicago, 2016.
[32] Eurocode 4. Design of Composite Steel and Concrete Structures. Brussels: European Committee for Standardization; 2004.
[33] CECS: 2018, Technical Standard for Structures with Concrete-Filled Multicellular Steel Tube Walls (Draft), China Association for Engineering Construction Standardization, 2018.

Table 1 Details of SCSSCW-ECs

Item	t_c (mm)	t_s (mm)	S_{v1} (mm)	S_{v2} (mm)	S_{h1} (mm)	S_{h2} (mm)	S_{va} (mm)	S_{ha} (mm)	f_y (MPa)	f_u (MPa)	E_{s1} (GPa)	σ_y (MPa)	σ_u (MPa)	E_{s2} (GPa)	f_c (MPa)
DW1-1	119.5	2.9	37	90	90	140	90	115	332	467	202	310	448	202	54.4
DW1-2	117.3	2.9	37	90	90	140	90	115	332	467	202	310	448	202	54.4
DW2[28]	117.9	3.0	65	115	62	115	90	115	235	349	201	235	365	202	54.4
DW3[28]	119.1	4.8	37	90	90	140	90	115	255	372	203	235	365	202	54.4
DW4	116.7	5.6	37	90	90	140	90	115	324	451	202	310	448	202	54.4
DW5-1	118.7	3.0	37	90	90	140	90	115	332	467	202	310	448	202	45.6
DW5-2	120.3	2.8	37	90	90	140	90	115	332	467	202	310	448	202	45.6
DW6[28]	116.0	2.9	77	130	90	140	130	115	235	349	201	235	365	202	54.4
DW7	116.4	3.1	117	170	90	140	170	115	332	467	202	310	448	202	54.4
DW8[28]	118.2	3.0	37	90	150	200	90	175	235	349	201	235	365	202	54.4
DW9	118.9	3.2	37	90	240	290	90	265	332	467	202	310	448	202	54.4

t_c and t_s denote thickness of concrete and steel faceplate, respectivley; S_{v1}, S_{v2}, S_{h1}, and S_{h2} denote the vertical and horizontal distance as shown in Fig. 4, respectivley; S_{va} and S_{ha} denote average vertical and horizontal distance of of C-channel connectors, respectivley; f_y and f_u denote yield and ultimate strength of steel faceplate, respectivley; σ_y and σ_u denote yield and ultimate strength of C-channel connectors, respectivley; f_c and f_{cu} denote cylindrical and cubic compressive strength of concrete, respectivley; E_{s1} and E_{s2} denote modulus of elasticity for steel faceplate and C-channel connectors, respectively.

Table 2 Test results and predictions by different methods of SCSSCW-ECs

Item	K_e (kN/mm)	Δ_u (mm)	$\Delta_{85\%}$ (mm)	*DI* Ratio	P_u (kN)	N_u (kN)	P_u / N_u	N_{uA} (kN)	P_u / N_{uA}	N_E (kN)	P_u / N_E	N_{CN} (kN)	P_u / N_{CN}
DW1-1	1723	3.82	5.25	1.37	4824	4846	1.00	4168	1.16	4405	1.10	4797	1.01
DW1-2	1750	4.27	5.28	1.24	4489	4802	0.93	4118	1.09	4356	1.03	4735	0.95
DW2[26]	1662	3.99	4.76	1.19	4312	4867	0.89	3873	1.11	4108	1.05	4479	0.96
DW3[26]	1939	3.58	5.22	1.46	6016	5573	1.08	4526	1.33	4752	1.27	5089	1.18
DW4	2158	3.99	4.68	1.17	5971	6193	0.96	5107	1.17	5344	1.12	5636	1.06
DW5-1	1460	3.25	5.29	1.63	3991	4266	0.94	3695	1.08	3892	1.03	4217	0.95
DW5-2	1591	3.84	6.87	1.79	3926	4226	0.93	3692	1.06	3889	1.01	4224	0.93
DW6[26]	1653	3.46	4.02	1.16	4183	4357	0.96	3788	1.10	4024	1.04	4387	0.95
DW7	1605	2.89	3.52	1.22	4226	4214	1.00	4169	1.01	4406	0.96	4775	0.89
DW8[26]	1740	3.08	3.61	1.17	4409	4506	0.98	3882	1.14	4116	1.07	4489	0.98
DW9	1783	2.79	3.53	1.27	4283	4403	0.97	4282	1.00	4518	0.95	4898	0.87
Mean							0.97		1.11		1.06		0.98
Cov							0.05		0.09		0.09		0.09

K_e denotes initial stiffness; Δ_u and $\Delta_{85\%}$ denote displacement at P_u and 85% P_u; *DI* Ratio denotes ductility ratio; P_u denote experimental ultimate compressive resistance; N_u, N_{uA}, N_{uE} and N_{CN} denote the predicted ultimate compressive resistance by TM, AISC 360-16, Eurocode 4 and CECS 2018.

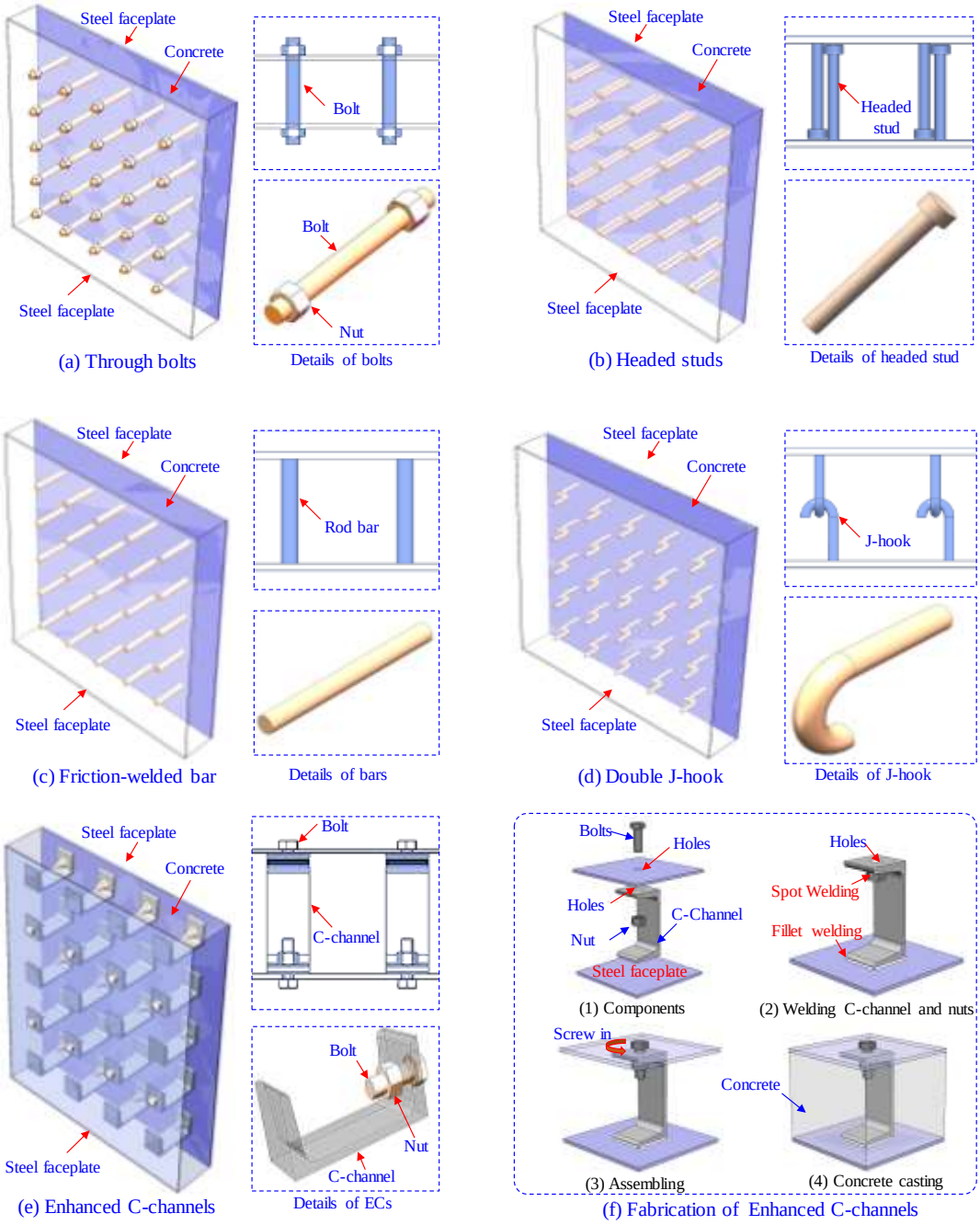

Fig. 1 SCSSCWs with different bonding connectors

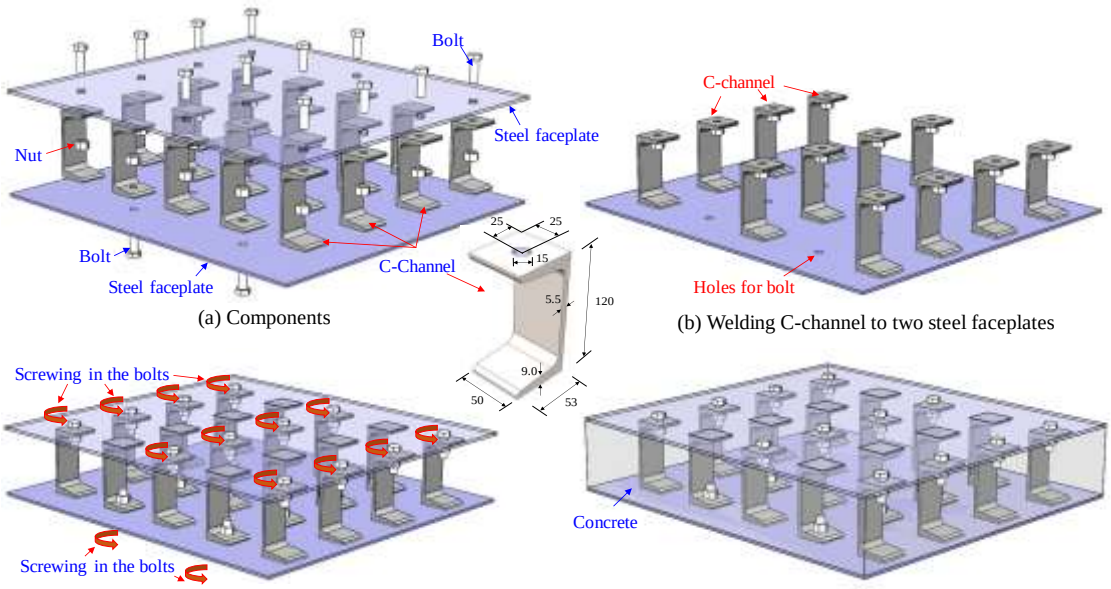

(a) Components (b) Welding C-channel to two steel faceplates

(c) Assembling the two steel faceplates by bolt (d) Concrete casting

Fig. 2 Details of fabrication procedures for SCSSCW-ECs

(a) Preparing steel skeleton (c) Concrete casting

(b) Preparing mould for concrete casting (d) SCSSCW-ECs after casting

Fig. 3 Fabrication of SCSSCW-ECs specimens for testing

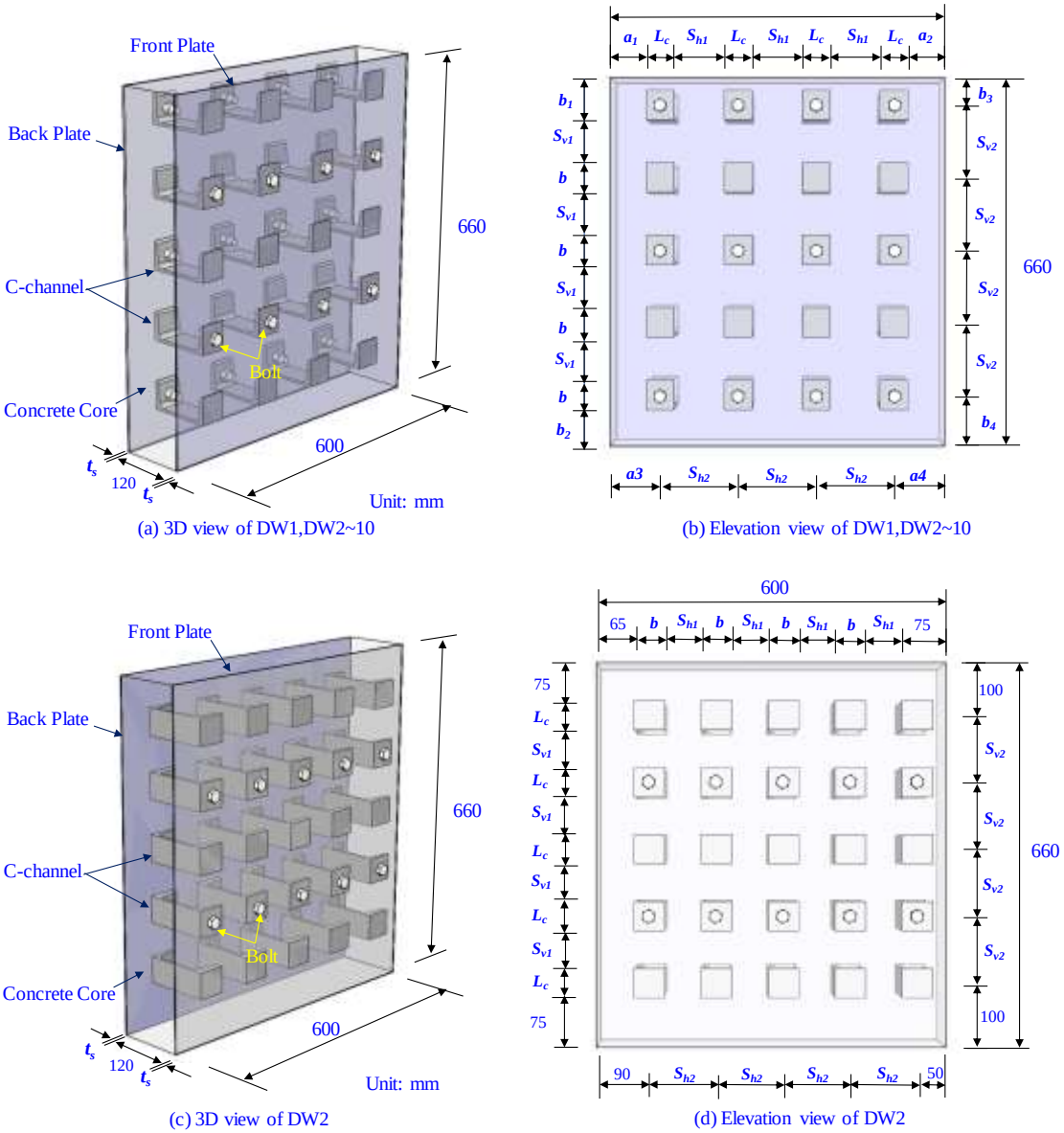

Fig. 4 Geometric details of SCSSCW specimens in the testing program

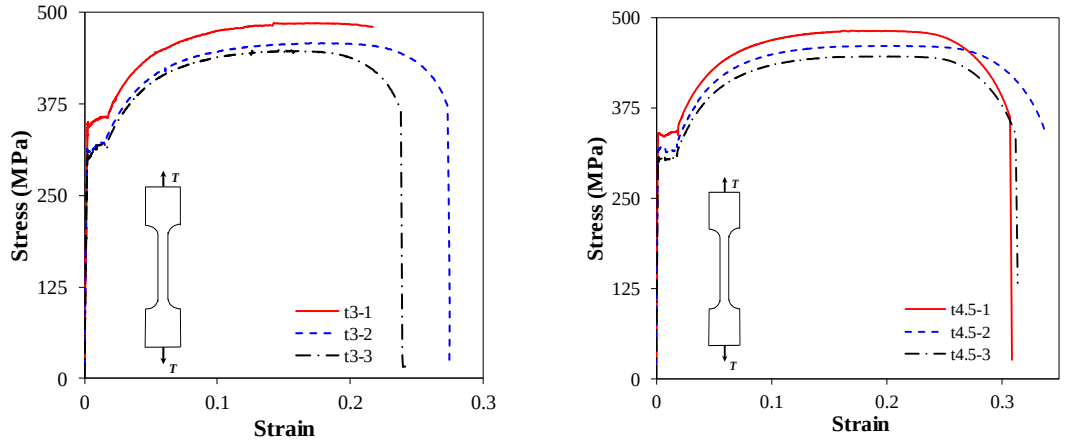

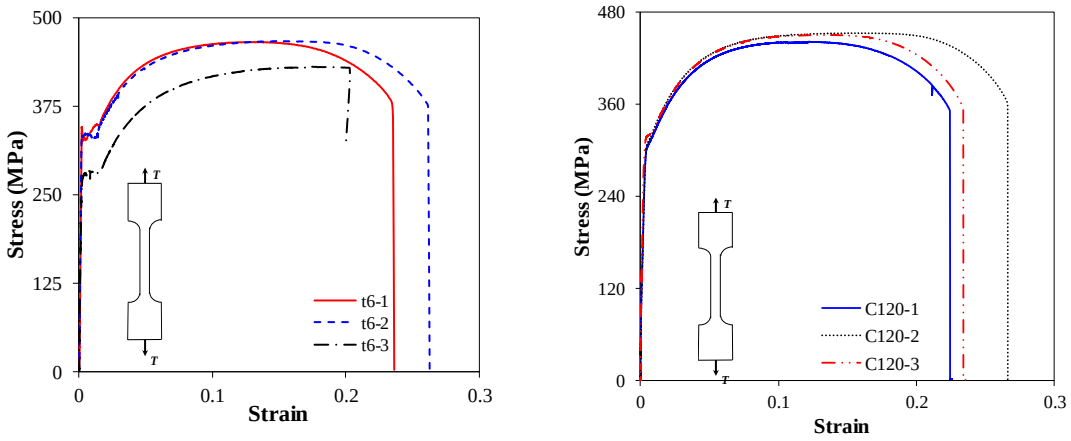

(c) 6mm-thick steel plate (d) C-channel

Fig. 5 Tensile stress-strain curves of steel faceplates and C-channels

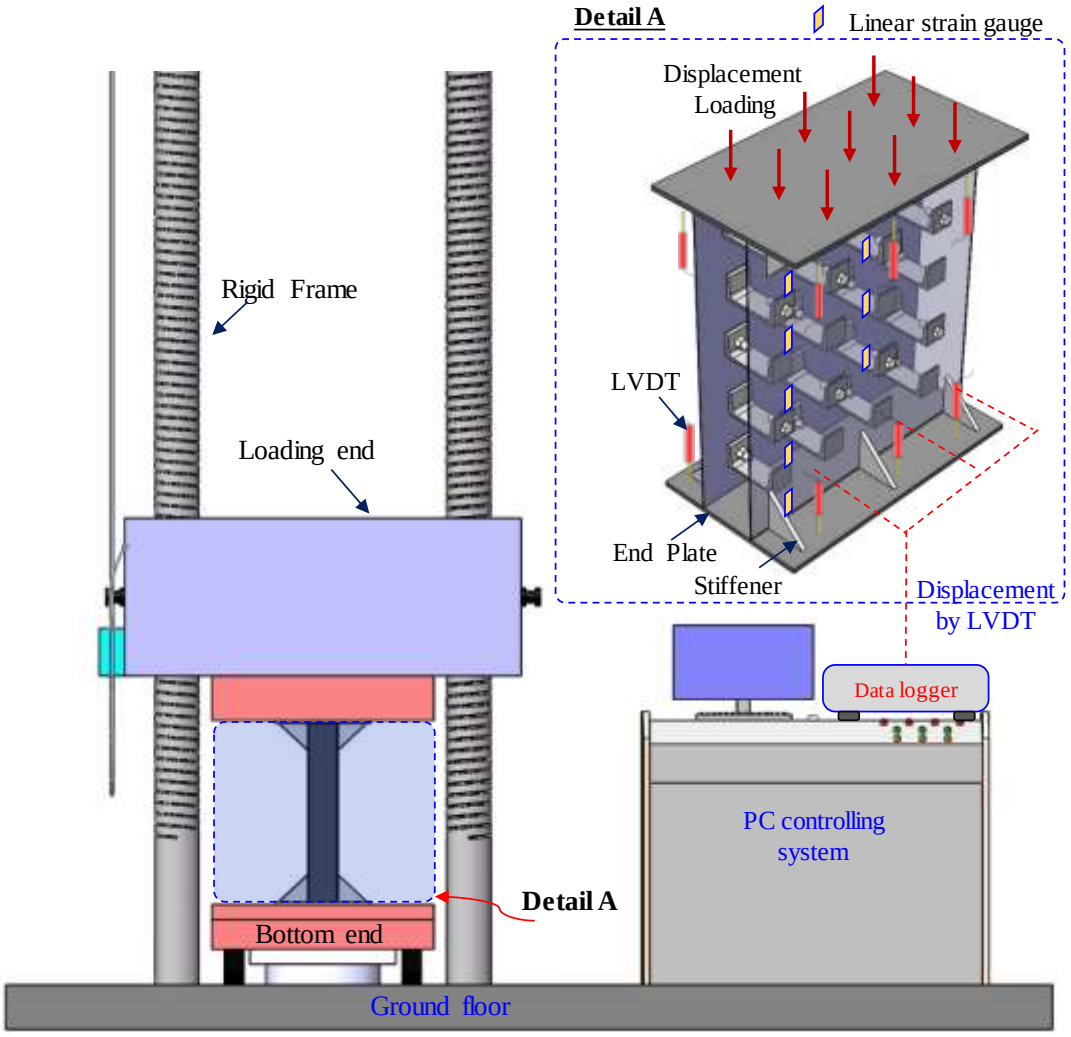

Fig. 6 Setup of compression tests on SCSSCW-ECs

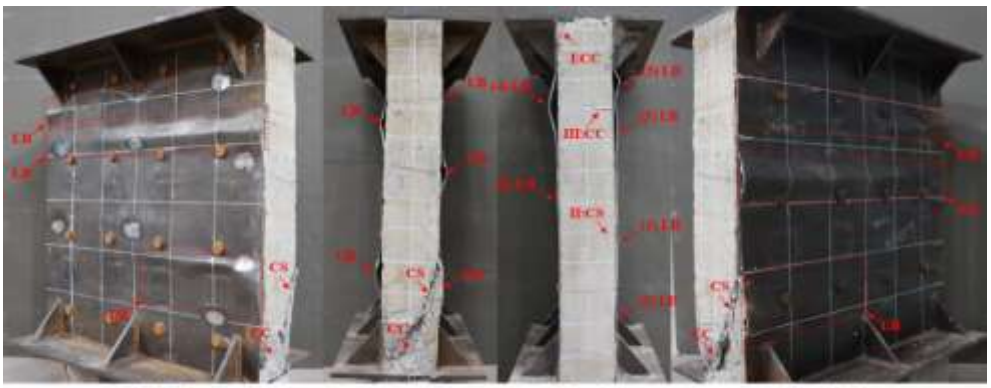

Left side view Front view Back view Right side view

(a) DW1-1

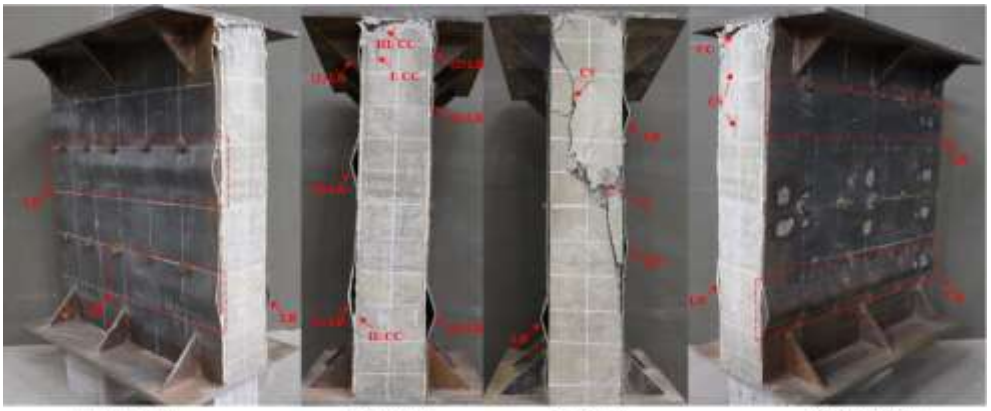

Left side view Front view Back view Right side view

(b) DW2

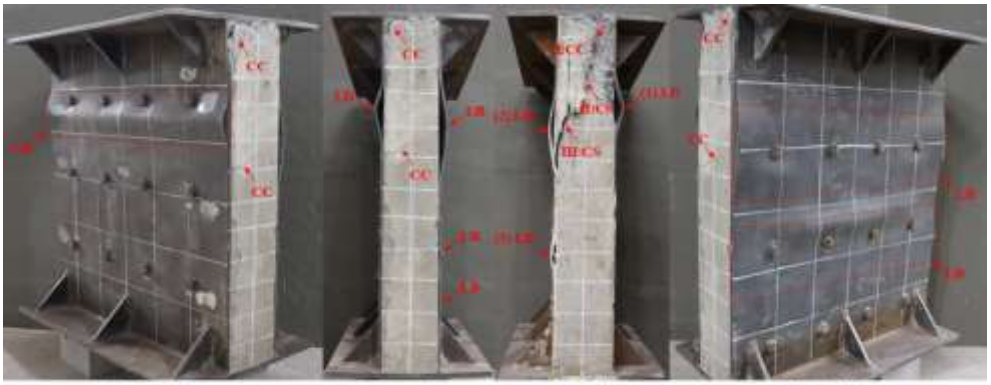

Left side view Front view Back view Right side view

(c) DW4

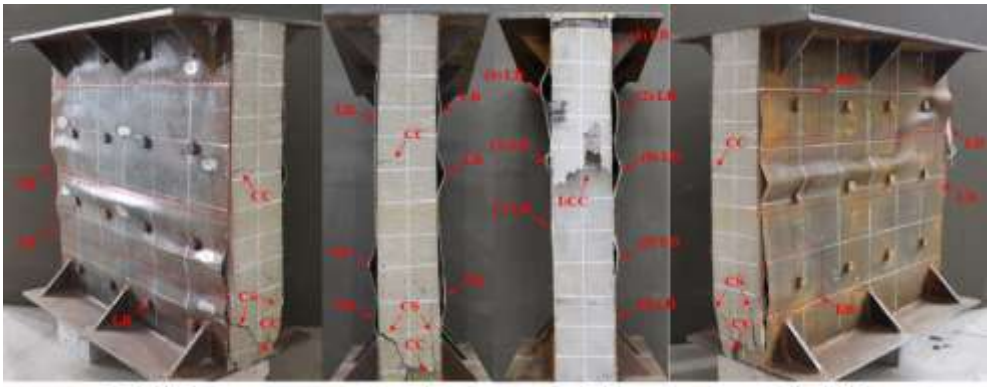

Left side view Front view Back view Right side view

(d) DW5-1

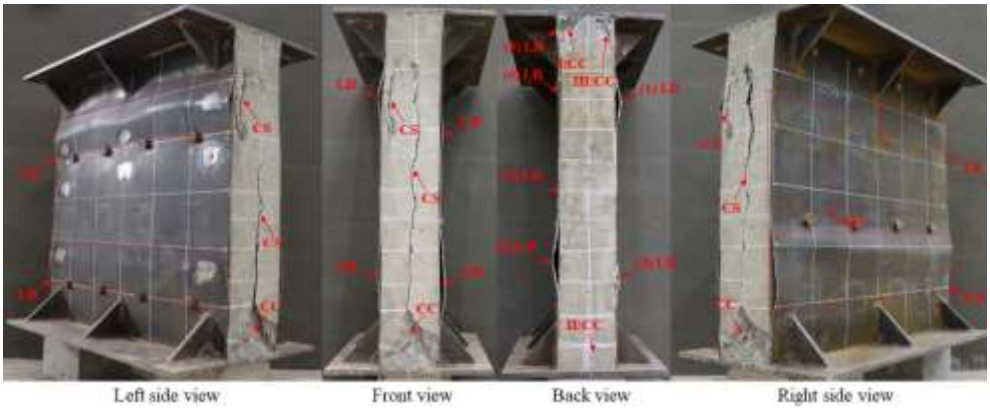

(e) DW7

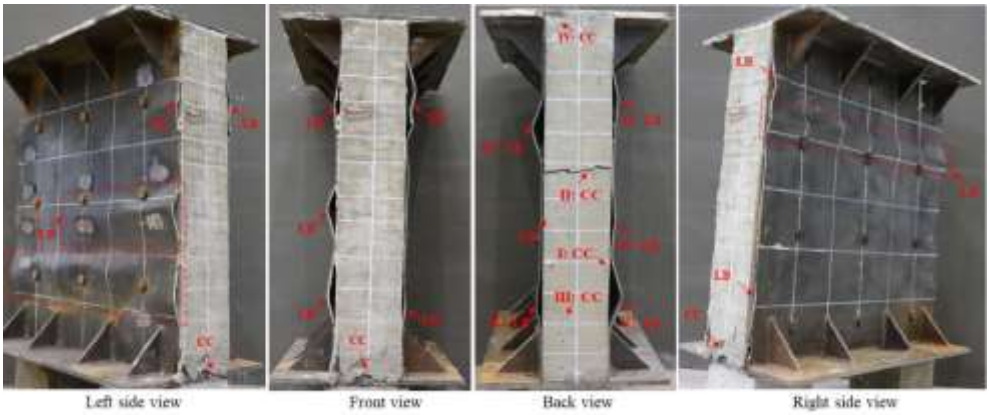

(f) DW8

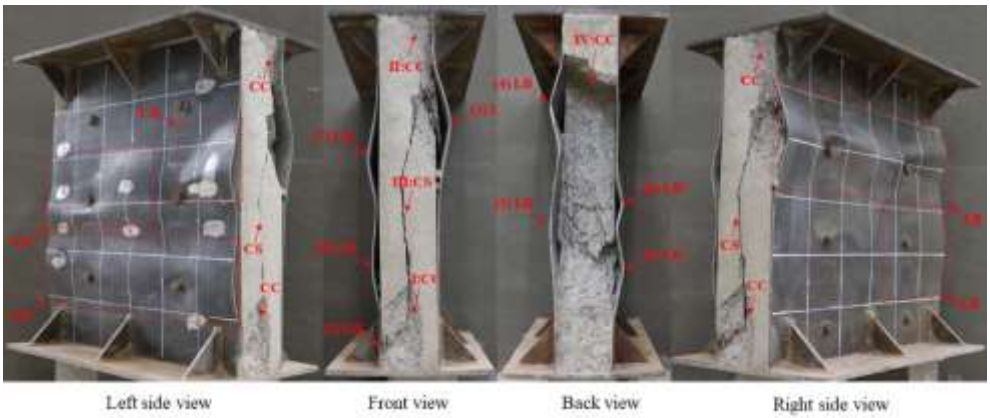

(g) DW9

Fig. 7 Failure modes of SCSSCW-ECs (LB, local buckling; CC, concrete crushing; CS, concrete splitting)

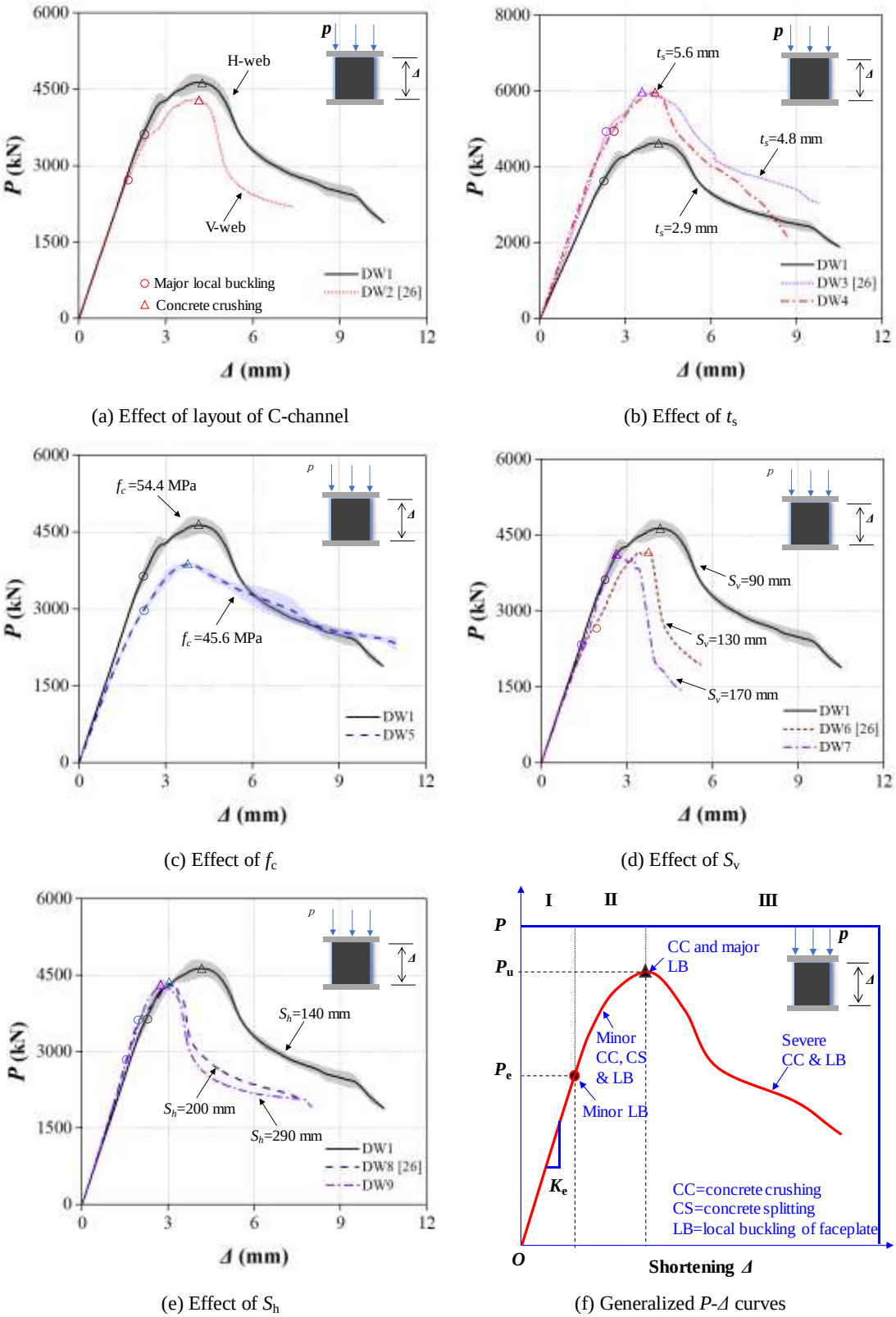

(a) Effect of layout of C-channel

(b) Effect of t_s

(c) Effect of f_c

(d) Effect of S_v

(e) Effect of S_h

(f) Generalized *P-Δ* curves

Fig. 8 Load versus shortening curves of SCSSCW-ECs subjected to compression

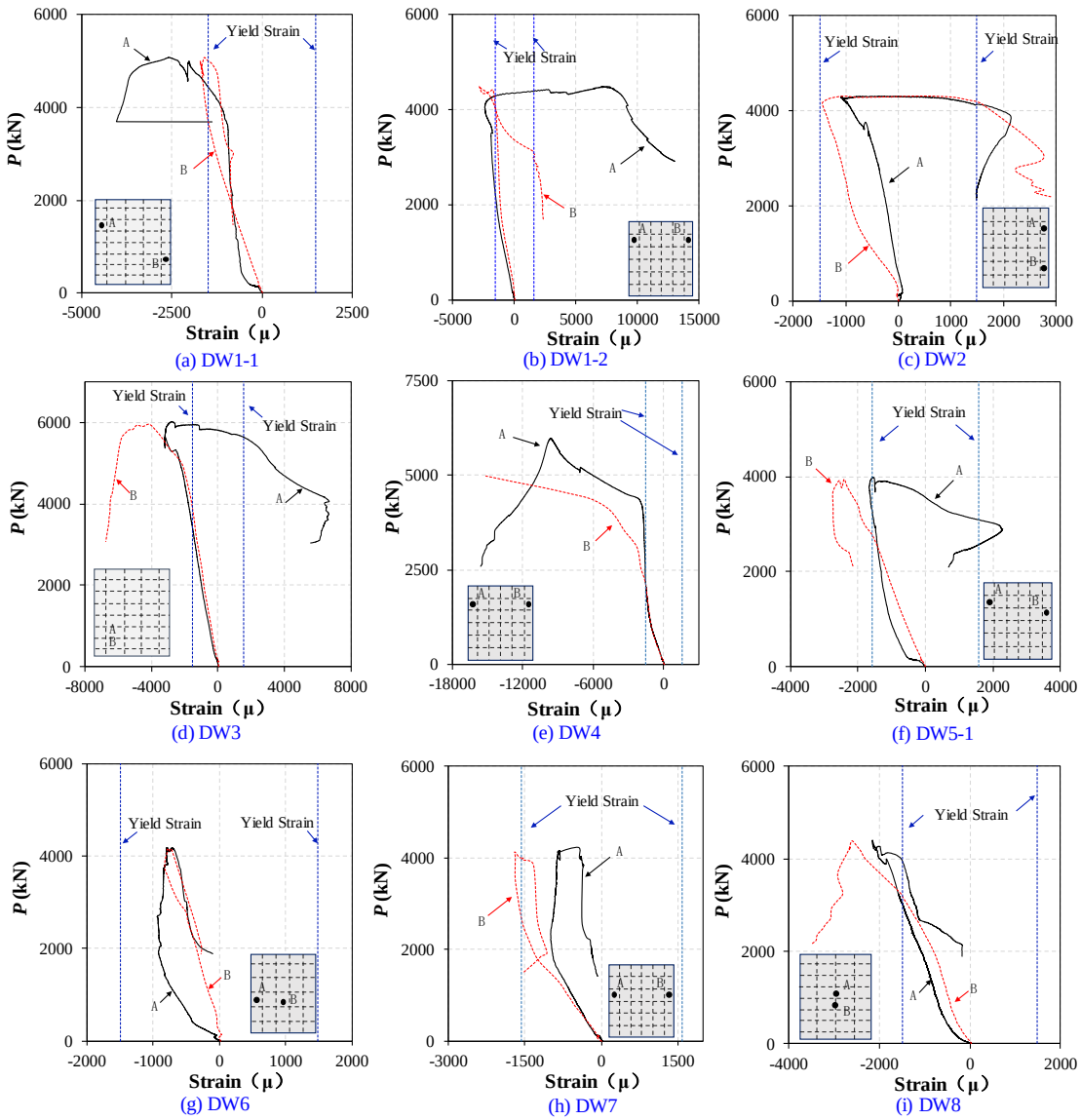

Fig. 9 Load versus strain curves for steel faceplates

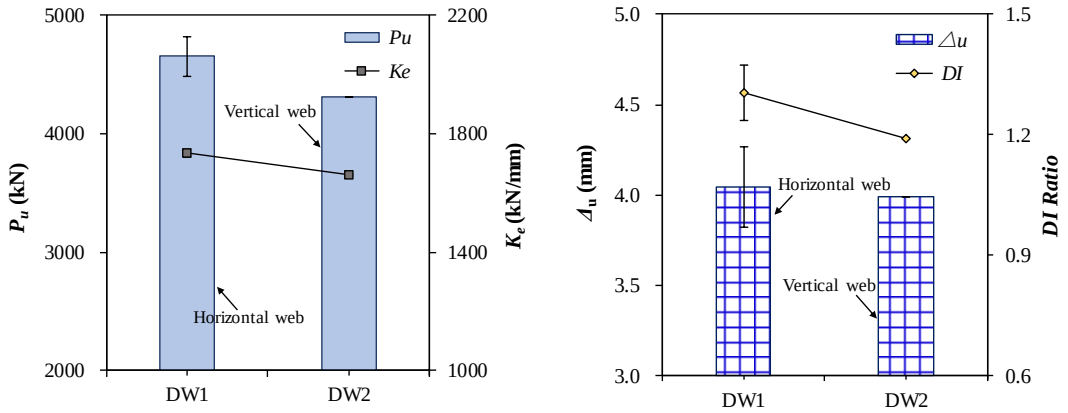

(a) Effect of layout of C-channel on strength

(b) Effect of layout of C-channel on ductility

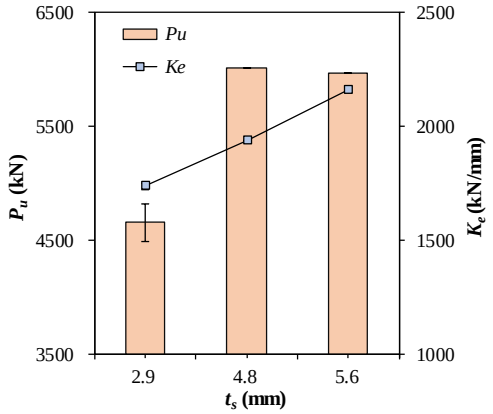

(c) Effect of t_s on strength

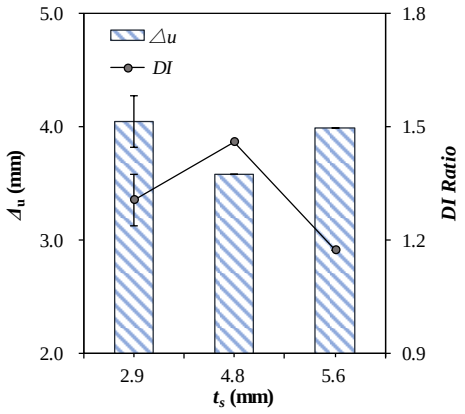

(d) Effect of t_s on ductility

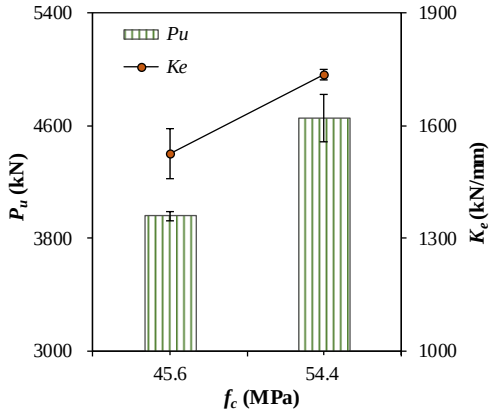

(e) Effect of f_c on strength

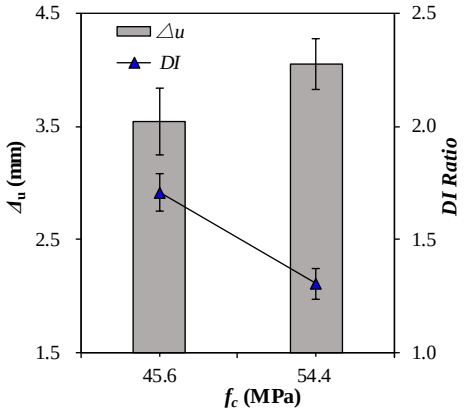

(f) Effect of f_c on ductility

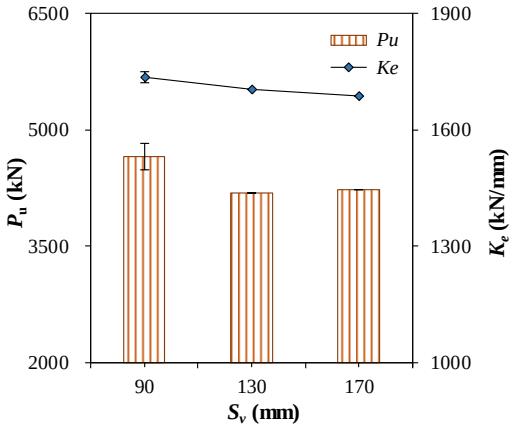

(g) Effect of S_v on strength

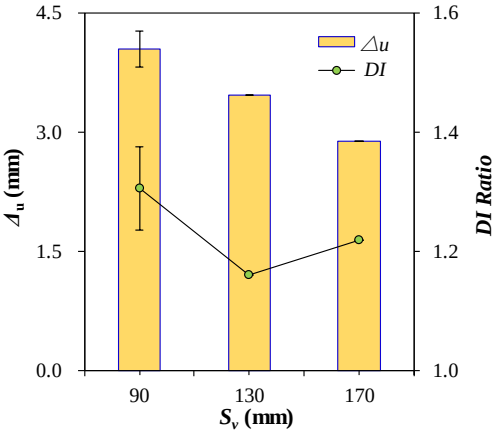

(h) Effect of S_v on ductility

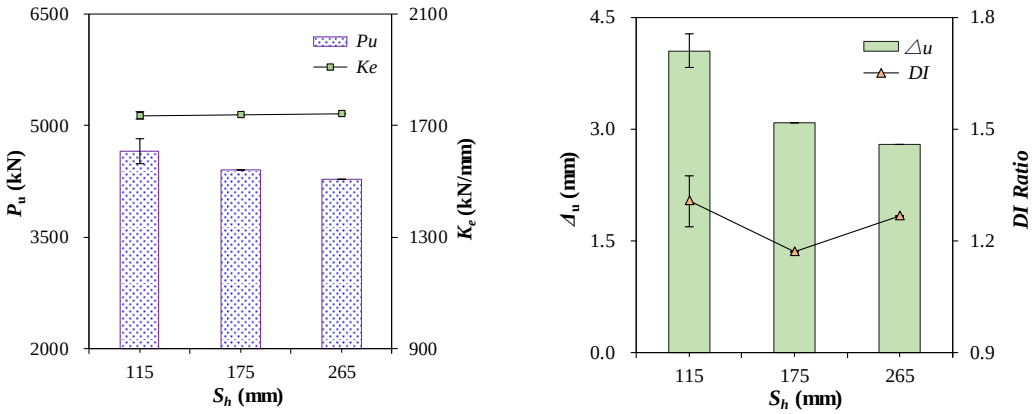

(i) Effect of S_h on strength (j) Effect of S_h on ductility

Fig. 10 Influences of different parameters on strength and ductility of SCSSCW-ECs

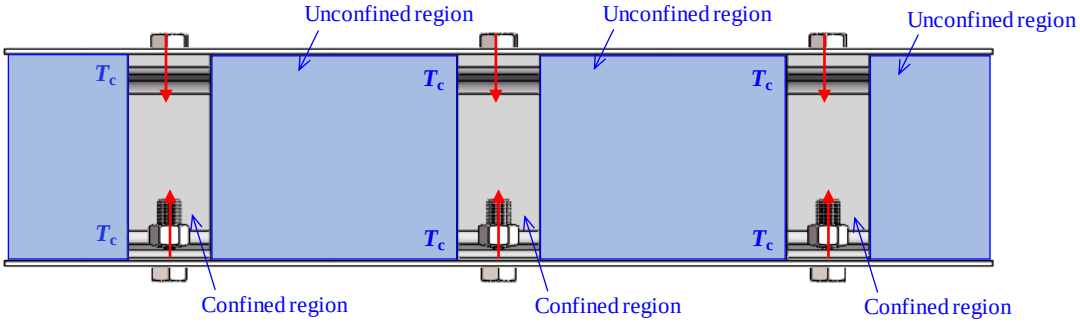

Fig. 11 Illustration on the confinement of C-channels on the concrete core in the cross section of SCSSCW-ECs

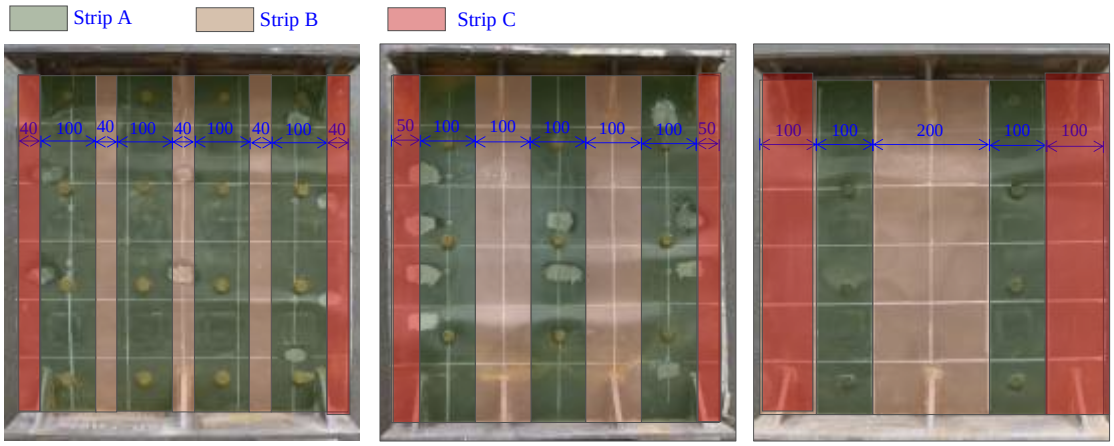

S_v=90 mm, S_h=115 mm (a) DW1

S_v=90 mm, S_h=175 mm (b) DW8

S_v=90 mm, S_h=265 mm (c) DW9

Fig. 12 Different buckling length of faceplate strips in SCSSCW-ECs

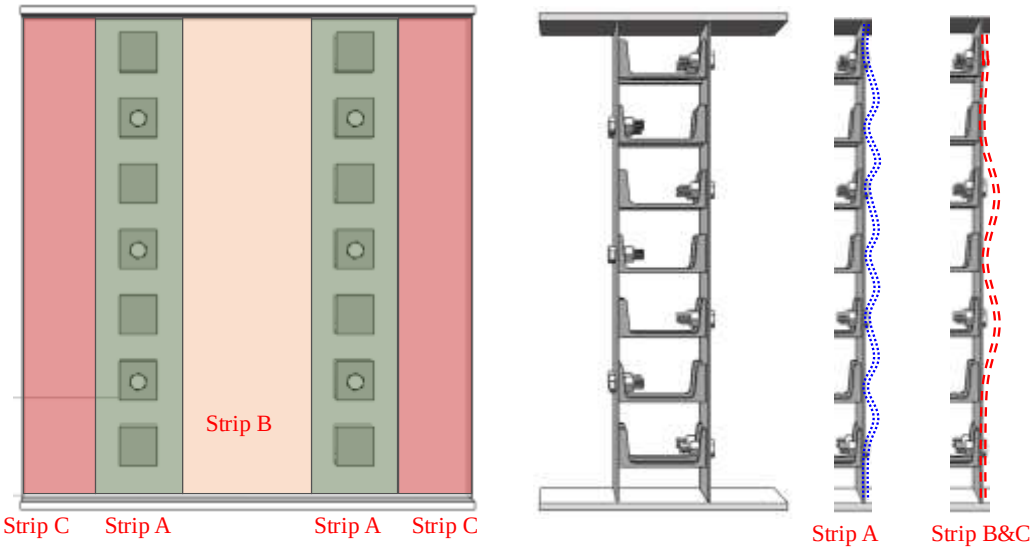

(a) Different strips in faceplate (b) Buckling mode for different strips

Fig. 13 Buckling modes for different strips in faceplates

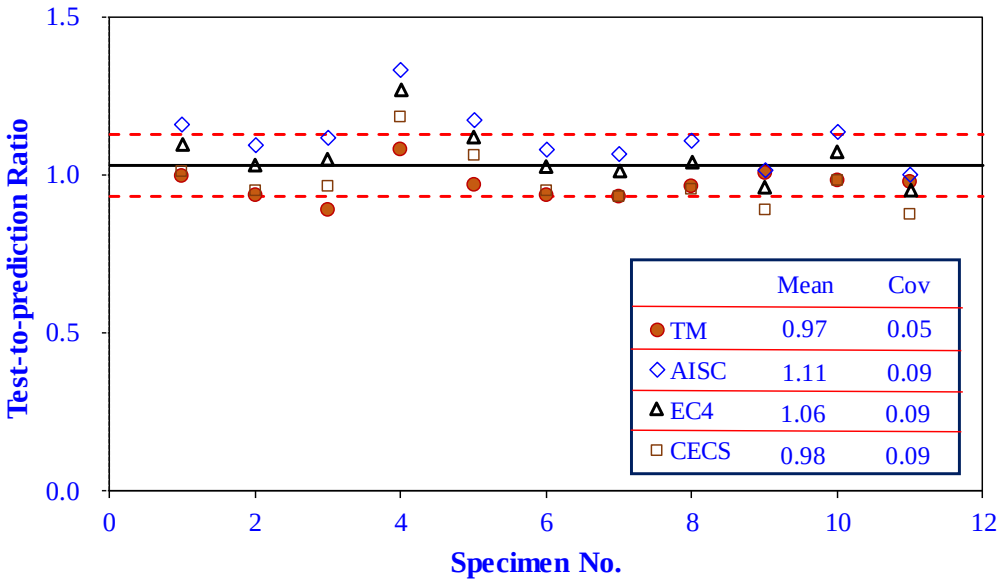

Fig. 14 Scatters of test-to-prediction ratios by different prediction methods